Potentials of Ultra-Short-Pulse Time-Domain Scattering Measurements

W. A. van Cappellen[1], R. V. de Jongh[1], and L. P. Ligthart[2]

[1]Signaal Delft
PO Box 90, 2600 AB Delft, The Netherlands
Tel: +31 15 2517800; Fax: +31 15 2517801; E-mail: wa.vancappellen@signaal.nl; rv.dejongh@signaal.nl

The work was performed at:

[2]International Research Centre for Telecommunications–transmission and Radar (ICTR)
Faculty of Information Technology and Systems, Delft University of Technology
Mekelweg 4, 2628 CD Delft, The Netherlands
Tel: (+31) 15-2781034; Fax: (+31) 15-2784046
E-mail: l.p.ligthart@its.tudelft.nl

Abstract

This article illustrates the potentials of ultra-short-pulse time-domain scattering measurements, and describes a facility to perform such measurements. The main advantages of measuring in the time domain are the high range resolution and the relatively simple measurement setup. A time-domain radar cross section measurement of a flat plate is performed, to illustrate the advantages of such methods over a conventional frequency-domain setup. The measurement was performed with a sampling oscilloscope, a pulse generator, and two 2-12 GHz ridged-horn antennas. Because the horns were not designed for transmitting transient signals, an additional system-response measurement, in combination with a software deconvolution algorithm, restored the impulse response of the object under test. Further processing separated the response of the object from clutter. A comparison of the time-domain data with calculated and measured frequency-domain radar cross sections shows good agreement. The high range resolution (100 ps) enabled the separation of scattering mechanisms (i.e., reflection, single and multiple diffraction). It is concluded that ultra-short-pulse time-domain measurements could be very beneficial.

Keywords: Time domain measurements; time domain analysis; radar cross sections; radar measurements; corrugated horn antennas; electromagnetic transient scattering; pulse measurements; transient response; pulse excited antennas

1. Introduction

The measurement of electromagnetic scattering has a large number of applications, ranging from model verification to as a design tool for ships, aircraft, and antennas. These measurements are usually performed in the frequency domain. The International Research Centre for Telecommunication–transmission and Radar (IRCTR) operates such frequency-domain facilities [1, 2]. Recently, IRCTR extended its facilities to perform ultra-short-pulse time-domain measurements [3]. In this method, the object under test is excited with an ultra-short pulse, instead of with a continuous or swept frequency. The resulting object response is measured with a sampling oscilloscope.

The main advantage of the time-domain technique is the large instantaneous bandwidth. The measurement of antenna characteristics with this technique has been successfully demonstrated [4]. For a number of years, the time-domain measurement technique has received increasing interest. This is reflected in the number of publications and books appearing on this subject [5]. The application of ultra-short pulses, in combination with a relatively high pulse amplitude, for time-domain antenna and radar cross section measurements, distinguishes the work at IRCTR.

This article describes the use of the time-domain facility to perform EM scattering measurements. A flat metal plate is measured by using pulses with a pulse width of 100 ps, offering a theoretical range resolution of 15 mm (after deconvolution). The large bandwidth allows identification of individual scattering sources on the object under test, and the separation of different scattering mechanisms [6]. For the flat plate, reflection and single and multiple diffraction are observed separately.

 1045-9243/2000/$10.00©2000 IEEE

2. Advantages and Limitations of Time-Domain Scattering Measurements

The work of IRCTR on time-domain scattering measurements is motivated by the potential advantages of the method. Advantages over the classical frequency-domain methods can be found on both the functional and operational level. On the functional level, we distinguish one distinct advantage:

- **High range resolution**. Instead of a single-frequency waveform, an ultra-short pulse illuminates the object under test. The large instantaneous bandwidth provides a very high range resolution, without any additional processing. For time-domain RCS measurements, the high range resolution offers the advantage of simple object diagnostics, and the possibility of resolving different scattering mechanisms. For example, in the setup described in this paper, the pulse width was 100 ps, offering a range resolution of 15 mm.

The method has a number of additional advantages on the operational level:

- **Direct gating**. Time gating is directly available. No additional processing is required, as in the frequency domain. Reflections outside the time window of interest are removed, without the introduction of errors.

- **Reduction of measurement time**. Time-domain scattering measurements can reduce the measuring time significantly, thereby reducing the use of scarce measurement facilities. This reduction is obtained from the large bandwidth provided in a single measurement. Additionally, the high range resolution allows simple diagnostics of the measurement environment. Interfering reflections can be traced, and are reduced with absorbers.

- **Simple measurement setup**. In general, the time-domain measurement setup is simpler and cheaper than is a frequency-domain setup.

The main limitation we observed in our measurements is the

- **limited signal-to-noise ratio**. The energy of the excited pulse is restricted by the pulse-generator hardware. The pulse-generator parameters are the result of a trade-off among amplitude, pulse width, and repetition rate. Improvement of the generator specifications is limited by the current state of technology. A possible solution can be the use of an ultra-wideband low-noise amplifier.

3. Formulation of Time-Domain EM Scattering

For time-domain scattering measurements, it is appropriate to use a time-domain formulation. In this section, this formulation is derived. The first part of this section summarizes the frequency-domain expressions, to show their equivalence with the time-domain expressions.

3.1 Formulation in the Frequency Domain

Figure 1 shows the setup for electromagnetic scattering measurements. The relationship between the transmitted and the received power is described by the radar range equation [7]:

$$\frac{P_r(f)}{P_t(f)} = \sigma \frac{G_t(f)G_r(f)}{4\pi}\left[\frac{\lambda}{4\pi R_1 R_2}\right]^2, \tag{1}$$

or

$$\sigma = \frac{P_r(f)}{P_t(f)} \frac{4\pi}{G_t(f)G_r(f)}\left[\frac{4\pi R_1 R_2}{\lambda}\right]^2, \tag{2}$$

where σ is the RCS of the object under test. P_r and P_t are known, and the system-response measurement provides the combined antenna gain, $G_t(f)G_r(f)$.

The unknown variables in the equation are the gain functions of the antennas. The product of these two gain functions can be determined with an additional experiment: the system-response measurement (Figure 2). The system-response measurement is described by the Friis transmission equation [8]:

$$\frac{P_r(f)}{P_t(f)} = \left(\frac{\lambda}{4\pi R}\right)^2 G_t(f)G_r(f). \tag{3}$$

In this equation, $P_t(f)$ and $P_r(f)$ represent the transmitted and the received powers, respectively. λ is the wavelength of the transmitted signal, and R is the range (the distance) between the two antennas. $G_t(f)$ and $G_r(f)$ are the gains of the transmitting and the receiving antenna. On the basis of these two measurements, the electromagnetic scattering characteristics of the object are determined.

3.2 Formulation in the Time Domain

To measure the time-domain scattering, a time-domain variant of the frequency-domain formulation is derived. In the time

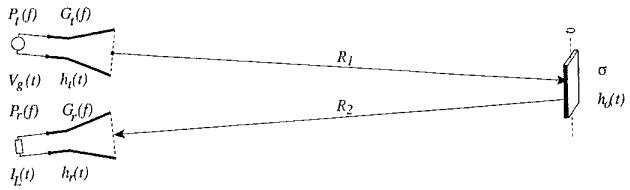

Figure 1. The setup for the scattering measurement.

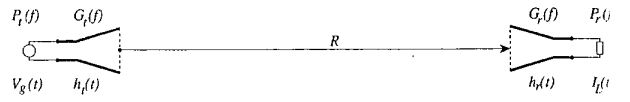

Figure 2. The setup for the system-response measurement.

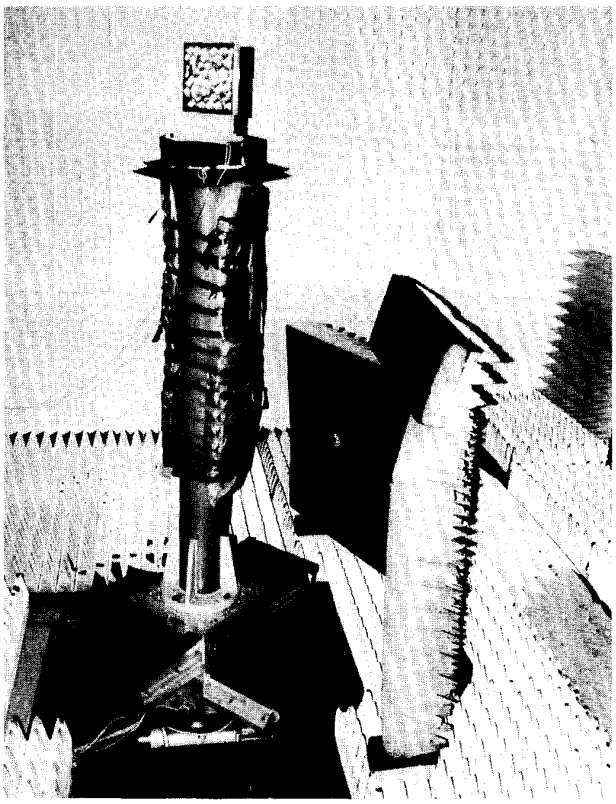

Figure 3. A photo of the pedestal with the object.

domain, it is more convenient to work with the generator voltage and the received antenna current (or voltage), instead of using the received and the transmitted power levels. For the setup given in Figure 2, Shlivinski et al. [9] derived an expression for the receiver antenna current in the time domain:

$$I_L(t) = \frac{1}{4\pi R}\frac{c^{-1}\eta}{2Z_{0T}Z_{0R}}\left\{\left[\mathbf{h}_t(\mathbf{r}_{TR},\cdot)*\mathbf{h}_r(\mathbf{r}_{RT},\cdot)\right]*V_g(\cdot)\right\}\left(\tau - t_g - t_L\right) \tag{4}$$

where $\eta = \sqrt{\mu/\varepsilon}$ is the free-space wave impedance, V_g is the generator-voltage waveform, Z_{0T} and Z_{0R} are the characteristic impedances at the transmitter and receiver, and $\mathbf{r}_{TR}$ and $\mathbf{r}_{RT}$ are the unit vectors from the transmitting antenna to the receiving antenna and vice versa, respectively. $\mathbf{h}_t$ and $\mathbf{h}_r$ are the effective heights of the transmitting and receiving antennas (the effective height is an equivalent of the antenna gain function for the time-domain, and can be considered to be the impulse response of an antenna). The last term in this expression, $\left(\tau - t_g - t_L\right)$, is an index of the convolution term between the square braces. The $\cdot$ is an arbitrary variable, and * denotes convolution.

The above expression for I_L is now expanded for the setup of Figure 1. First, the incident electric field at the object is determined. Then, a time-domain scattering function is defined, which is used to derive an expression for the load current.

The electric field at the object is [9]

$$\mathbf{E}(\mathbf{r},t) = -\frac{1}{4\pi R_1}\frac{c^{-1}\eta}{2Z_0}\left[V_g(\cdot)*\mathbf{h}_t(\mathbf{r},\cdot)\right]\left(\tau - t_g\right). \tag{5}$$

The time-domain scattering function, $h_o(t)$, is defined as the far-field impulse response of the object. Using this definition, the electric field at a distance R_2 from the object is

$$\mathbf{E}(\mathbf{r},t) = -\frac{1}{4\pi R_1}\frac{1}{4\pi R_2}\frac{c^{-1}\eta}{2Z_0}\left\{\left[V_g(\cdot)*\mathbf{h}_t(\mathbf{r},\cdot)\right]*\mathbf{h}_o(\mathbf{r},\cdot)\right\}\left(\tau - t_g\right). \tag{6}$$

The current due to this electric field is

$$I_L(t) = -\frac{1}{Z_0}\left[\mathbf{h}_r(\mathbf{r},\cdot)*\mathbf{E}(\cdot)\right]\left(\tau - t_L\right), \tag{7}$$

or

$$I_L(t) = \frac{1}{4\pi R_1}\frac{1}{4\pi R_2}\frac{c^{-1}\eta}{2Z_{0T}Z_{0R}}\left[\left\{\left[\mathbf{h}_t(\mathbf{r}_{TR},\cdot)*\mathbf{h}_r(\mathbf{r}_{RT},\cdot)\right]*\mathbf{h}_o(\mathbf{r},\cdot)\right\}*V_g(\cdot)\right]\left(\tau - t_g - t_L\right). \tag{8}$$

The (combined) antenna impulse response $h_a(t) = V_g(\cdot)*\left[\mathbf{h}_r(\mathbf{r}_{RT},\cdot)*\mathbf{h}_t(\mathbf{r}_{TR},\cdot)\right]\left(\tau - t_g - t_L\right)$ is determined from the system-response measurement.

The object impulse response, $h_o(t)$, is obtained by performing a deconvolution of the measured object response and the system response, $h_a(t)$.

4. Description of Time-Domain Radar Cross Section Measurements

To illustrate the potentials of time-domain scattering measurements, the radar cross section (RCS) of a flat plate is determined. Three measurements are performed to extract the scattering characteristics of the object under test:

A system-response measurement. The system-response measurement determines the transfer function or impulse response of the system.

A background-response measurement. The background-response measurement determines the clutter (empty-room scattering contributions and antenna coupling).

An object-response measurement. The object-response measurement determines the total scattered field.

All measurements are performed with vertical transmitter and receiver polarization.

4.1 System-Response Measurement

The system-response measurement determines the impulse response of the system, including the influences of the pulse gen-

erator, cables, antennas, and receiver. The antennas are mounted on two pedestals, separated by distance R, and satisfy the far-field condition (i.e., the radiated waves can be approximated by plane waves). This measurement is performed with exactly the same components as those used for the final RCS measurement. In the system-response measurement, we did not compensate for the (small) bistatic angle, thus introducing an error. Alternatively, the system response can be extracted from the measurement of a reference target (e.g., a flat plate).

4.2 Object-response measurement

The response of the object–including the clutter and cross coupling–is determined by the object-response measurement. The antennas are mounted with a bistatic angle of 6°. The object is located on a rotating pedestal (see Figure 3). The backscattering of the object is determined for various angles. After performing the object measurement, the measured background response is subtracted to remove stationary clutter. The result after subtraction is deconvolved with the system response to obtain the scattering of the object under test.

4.3 Background-Response Measurement

The background-response measurement determines the backscatter of the empty room, and the cross coupling between the transmitting and receiving antenna. Except for the object, the equipment is mounted in the same way as it is for the object-response measurement. Provided that the observed signals are stationary, these unwanted contributions can be removed from the object response by subtraction. For optimal stability, the background is measured just before or after the object-response measurement.

4.4 Description of the Measurement Equipment

The measurements were performed in the Delft University Chamber for Antenna Tests (DUCAT). DUCAT is a moderately sized shielded environment (shielding of at least 120 dB), of 3 × 3 × 6 meters. On the inside, the chamber is covered with absorbing material, to reduce scattering from the walls. The antennas and the object under test are positioned on two pedestals with a mutual distance of 3.5 m. The K2-63 time-domain measurement system is integrated in DUCAT, and consists of a sampling oscilloscope and a pulse generator.

4.4.1 Sampling Oscilloscope

The K2-63-1 sampling oscilloscope controls the measurement system. It provides the pulse generator with trigger pulses, and collects and displays the measured data. The bandwidth of the input channel is 0-18 GHz. To avoid time-scale inaccuracy, the time scale is calibrated with an internal reference signal (derived from a crystal oscillator) before every measurement. The data from the sampling scope are transferred to a PC and stored.

4.4.2 Pulse Generator

The pulse generator (K2-63-2), with an external pulse shaper, produces pulses with a 50% width of 85 ps and a peak voltage of 30 V, at a pulse repetition rate of 100 kHz (see Figure 4). In the early days of transient measurements, a major concern and deficiency was the pulse-to-pulse variability of the pulse generator. These variations introduced errors in the measured responses. Nowadays, the performance of the pulse generators has been improved, resulting in a better pulse-to-pulse stability. The stability of the K2-63-2 pulse generator has been measured and is expressed in its signal-to-noise ratio [3]. In our area of interest (from 2-12 GHz), its signal-to-noise ratio is above 90 dB.

4.4.3 Antennas

Ideally, transient antennas should be used to transmit and receive the ultra-short pulse, for example, TEM horns. They preserve the original pulse shape because they are ultra-wideband, and have a constant phase center. However, because these antennas were not available, two 2-12 GHz ridged-horn antennas were used. Their gain is specified to be from 15 dB at 2 GHz to 27 dB at 12 GHz. An additional system-response measurement, in combination with a software deconvolution algorithm, restores the impulse response of the object under test.

4.4.4 Object

The object under test is an aluminum plate, with one flat side and one artificially rough side. The size of the plate is 148 × 148 × 15.7 mm. Detailed information concerning the plate and the scattering from this plate (calculations and measurements) is provided by Pieper [10].

5. Signal Processing

The raw data are processed to obtain the scattering of the flat plate. The processing has two purposes:

1. clutter and cross-coupling suppression, and

2. resolution enhancement.

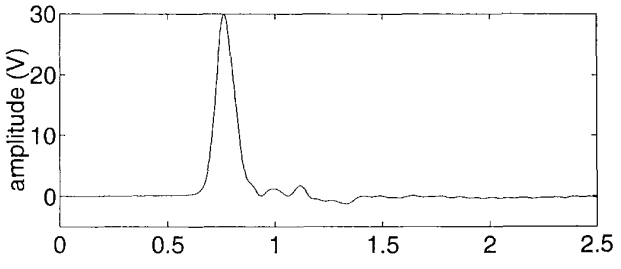

Figure 4. The time-domain signal at the pulse-shaper output.

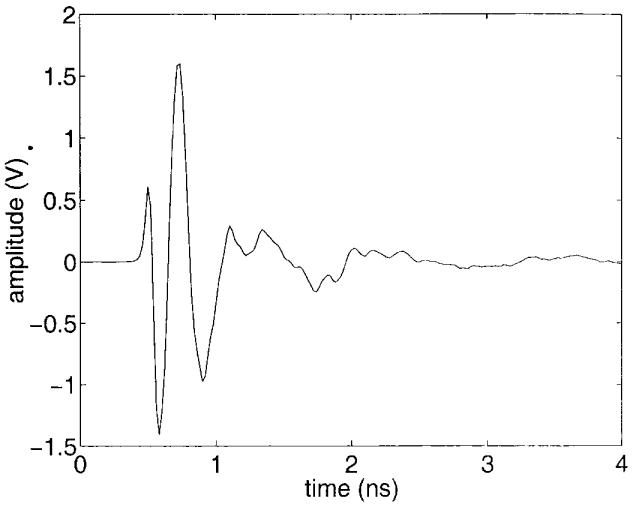

Figure 5. The measured system impulse response.

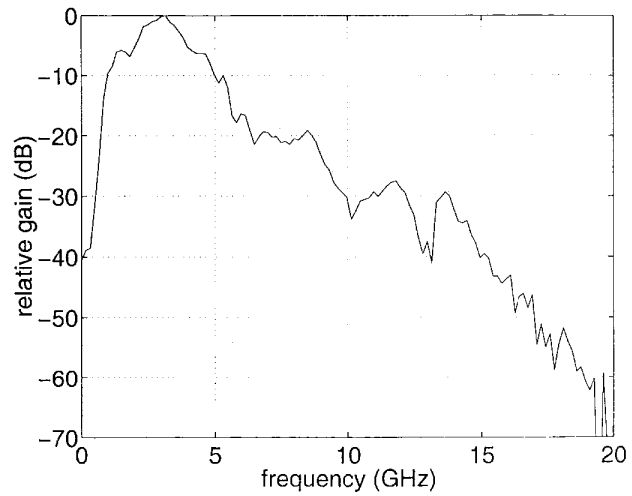

Figure 6. The calculated power spectrum of the system impulse response.

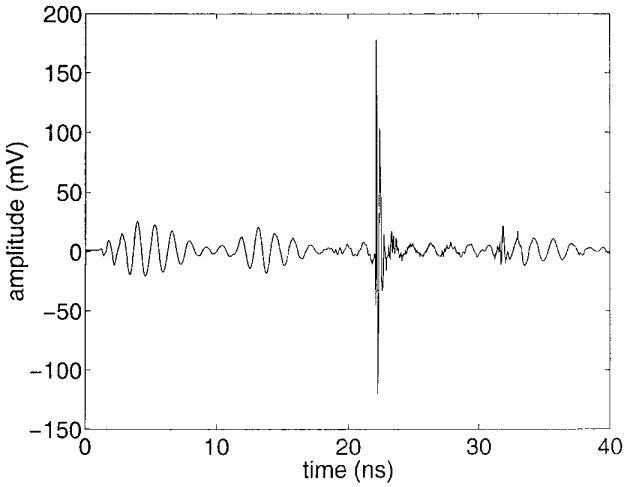

Figure 7. Time-domain results of the object-response measurement.

5.1 Clutter and Cross-Coupling Suppression

The RCS measurement of the flat plate is distorted by the clutter and cross-coupling of the antennas. Clutter is defined as the scattering contributions that do not originate from the object under test, for example, reflections from the walls of DUCAT or backscatter from the pedestal. Two techniques have been used in our experiments to remove the unwanted contributions: subtraction and gating. Cross-coupling from the transmitting to the receiving antenna can be removed with the same processing techniques. Interactions between the object and the environment (for example, when the scattered field is reflected via the walls to the receiving antenna) are gated out.

5.1.1 Subtraction

Assuming that clutter and cross coupling are stationary, their effect is reduced by the subtraction of the empty-room response from the object response. To minimize pulse drift and pulse-shape instability, the background response is measured directly before or after the object response is measured. If the background measurement and the object measurement are electromagnetically coupled, the subtraction will introduce additional errors. When the subtraction technique is used, one should be aware of its limitations. However, these limitations do not necessarily disturb the area of interest of the measurements: during the object-response measurement, part of the back wall is in the shadow region of the object, so there will be no scattering contribution from this part of the wall. During the background measurement, the object is removed, and the region directly behind it is illuminated by the antenna. When the background response is subtracted from the object response, we actually subtract too much. In our setup, this contribution is expected to be $2 \times 0.77/3 \times 10^8 = 5.1\,\text{ns}$ after the start of the plate response. This contribution turns out to be outside the time window of interest, and can thus be removed by time gating.

5.1.2 Gating

The second method used to remove clutter from the measurement is gating, or time-domain windowing. All contributions that do not overlap with the object response are ignored. These contributions include reflections on the RF cables, walls, and interaction of the object with the room.

5.2 Resolution Enhancement

A consequence of the usage of non-transient antennas is that the incident field at the object is not an infinitely short pulse. Consequently, the measured response is not the impulse response of the object. However, as shown in Section 3, the impulse response of the object can be reconstructed. This reconstruction, or pulse compression, is performed with a software deconvolution algorithm.

The deconvolution is implemented with a least-squares-based algorithm [11]. According to Hayward [12], this method gives

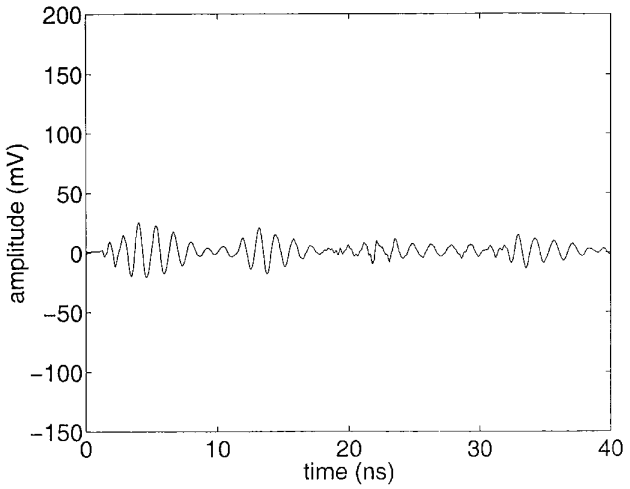

Figure 8. Time-domain results of the background-response measurement.

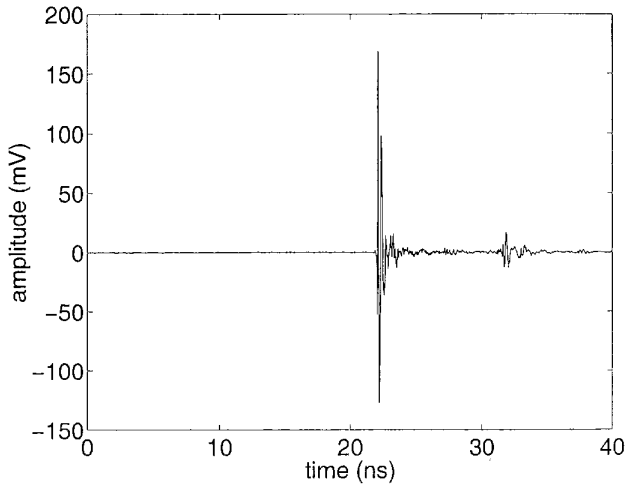

Figure 9. The time-domain object response after background subtraction.

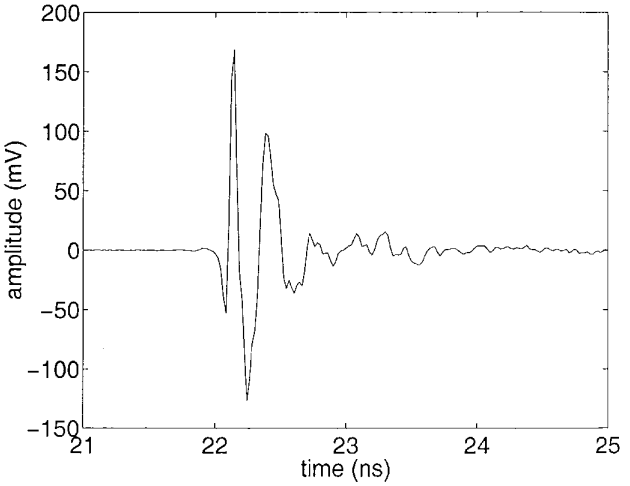

Figure 10. The gated time-domain object response after background-response subtraction.

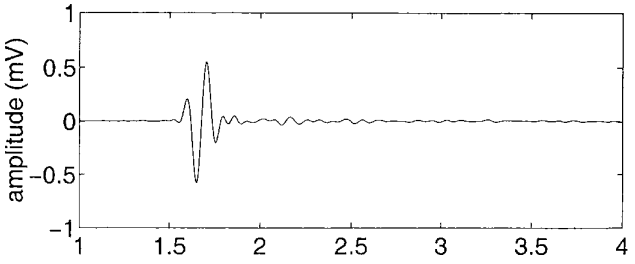

Figure 11. The result of the deconvolution performed on the signals of Figures 10 and 5 after bandpass filtering.

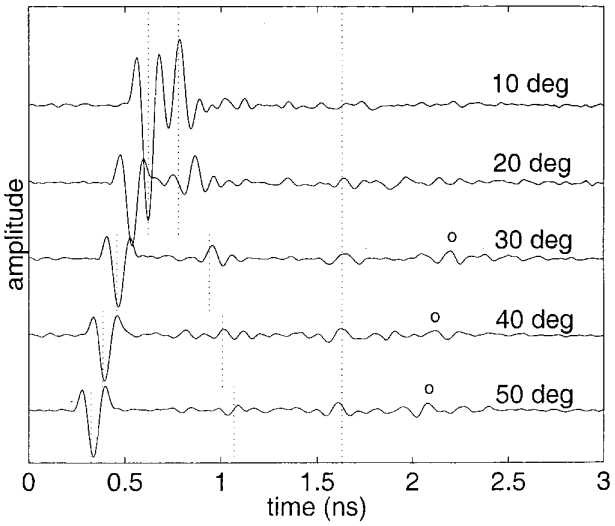

Figure 12. The processed flat-plate responses for rotation angles from 10° to 50°.

good results, even for relatively low signal-to-noise ratios. The algorithm determines the pseudoinverse of the antenna response with a singular-value decomposition. Each singular value corresponds to a small range of frequencies [13]. According to Rahman [14], satisfactory results are obtained when the number of singular values is proportional to the (estimated) signal-to-noise ratio of the input signal. Every singular value that is smaller than the value of the largest singular value, divided by the signal-to-noise ratio, is ignored.

A software bandpass filter is applied to the deconvolved result to remove all contributions that are outside the antenna bandwidth.

6. Discussion of the Measurement Results

This section discusses the results of the time-domain RCS measurements of a flat plate. The results are compared with predicted and measured frequency-domain results of the same plate.

6.1 Time-Domain Results

The time-domain signals are measured with a sampling time of 20 ps for all measurements.

6.1.1 System Transfer Measurement

The result of the system-transfer measurement is shown in Figure 5. The consequence of using non-transient antennas is that the original pulse shape is distorted. The main part of the response of the antennas that was measured has only a few oscillations, indicating a large bandwidth. The early-time response is followed by some trailing oscillations, which only contain energy at (relatively low) resonant frequencies. The dominant frequency of the tail is 900 MHz, which corresponds to the cutoff frequency of the horn antennas.

The power spectrum of the complete system impulse response is shown in Figure 6.

6.1.2 Object Measurement

The result of the broadside object measurement is shown in Figure 7. The relatively low frequency components are caused by cross-coupling between the two antennas. The large response after 22 ns is the backscatter of the object. The signal between 30 and 35 ns is caused by multiple reflections in the RF line. Around 18 ns, before the start of the object response, a second high-frequency backscatter signal can be observed. We determined experimentally that this reflection was caused by the sheets of absorber in front of the antenna (see Figure 3).

6.1.3 Background-Response Measurement

The result of the background-response measurement is shown in Figure 8. The scattering of the object has disappeared, but the direct coupling between the antennas and the room reflections are unchanged with respect to the object measurement.

6.1.4 Result After Background Subtraction

Figure 9 shows the complete time window of the measured object response, from which the background response is subtracted. The clutter and cross coupling are eliminated almost completely. The remaining signals are the object response, starting at 22 ns, and the first reflection on the RF cables, at 33 ns. Additionally, the error caused by shadowing is observed between 25 and 30 ns. Figure 10 shows a close-up of the object response.

6.1.5 Result After Deconvolution

Figure 11 shows the results after the deconvolution of the signals in Figure 10 and Figure 5. When we compare Figures 10 and 11, we can observe a significant improvement in resolution. The deconvolution results are shown for different angles of rotation of the flat plate in Figure 12. Note that the signals are plotted on various DC offset levels. The scattering mechanisms are explained by means of Figures 11 and 12.

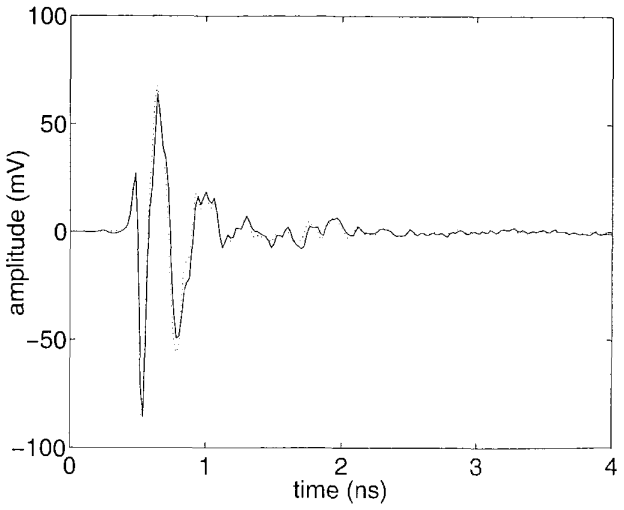

Figure 13. A comparison of the object response (dotted) and the numerically differentiated, amplitude-scaled-and-shifted antenna response (solid).

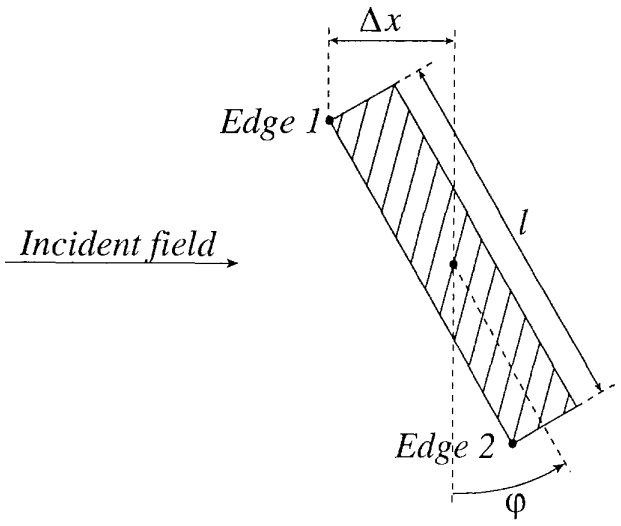

Figure 14. The distance, Δx, as a function of the azimuth angle, φ.

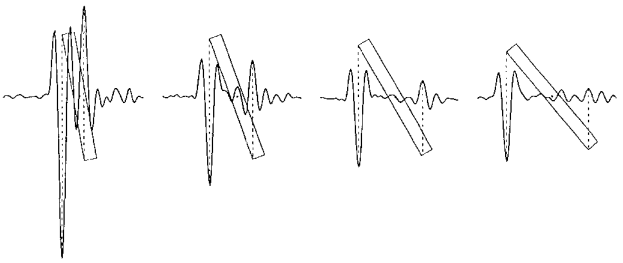

Figure 15. The calculated and measured positions of the leading- and trailing-edge diffraction.

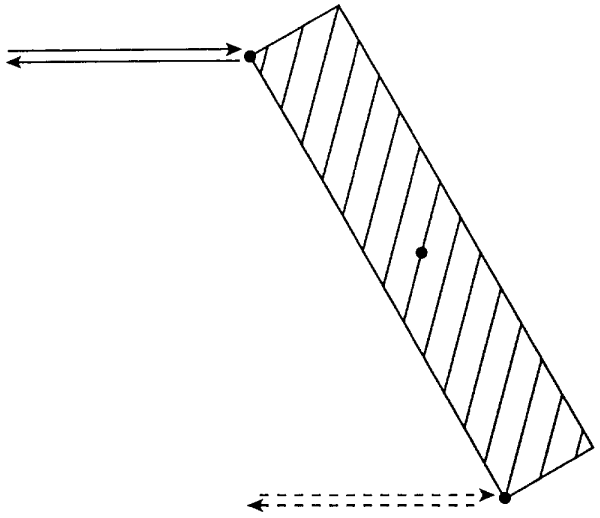

Figure 16a. An illustration of a single diffraction mechanism.

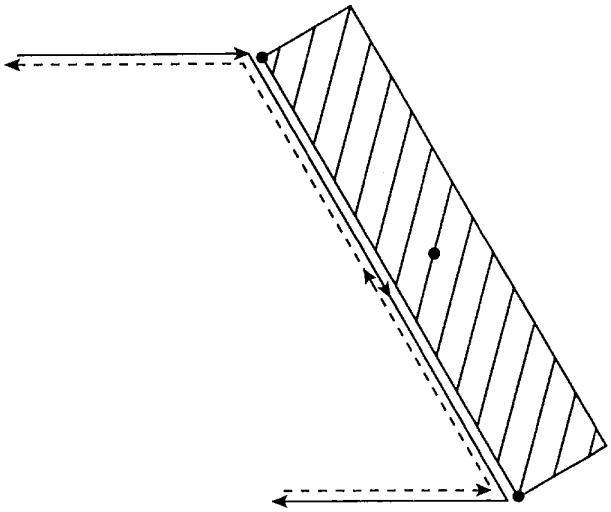

Figure 16b. An illustration of a double diffraction mechanism.

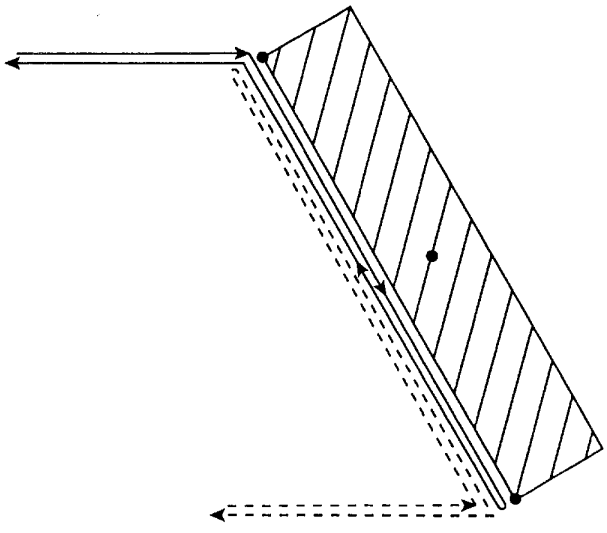

Figure 16c. An illustration of a triple diffraction mechanism.

6.1.5.1 Specular reflection. The backscattered signal is primarily determined by specular reflection for a rotation angle of 0° (broadside incidence). In the frequency domain, the specular reflection of a flat plate is proportional to the frequency. In the time domain, this relation corresponds to a differentiation. To verify this, the object response (Figure 10) is compared to the numerically differentiated, scaled and shifted antenna response in Figure 13. An excellent agreement between the curves is noted.

6.1.5.2 Single diffraction. The reflection contribution decreases rapidly when the flat plate is rotated. The edge diffraction of the incident field increases and becomes dominant. At 10° of rotation, the first negative (and largest) peak occurs: it is interpreted as the backscatter from the leading edge of the flat plate (edge 1 in Figure 14). The largest positive peak is the backscatter from the trailing edge.

The time delay between the leading and trailing edge is related to the difference in length of the propagation path. The delay increases as the rotation angles increase. With goniometric relations (Figure 14), the time delay for different rotation angles can be calculated. The short dotted lines in Figure 12 represent the predicted positions of the edge diffraction. The positions of the calculated and measured peaks correspond exactly (i.e., up to the sampling interval of 20 ps).

6.1.5.3 Multiple diffraction. The various types of multiple diffraction are identified by examining the length of their propagation paths (Figure 16). The doubly diffracted field has a constant delay, compared to a reference plane in front of the plate, for all rotation angles. The triply diffracted field has a constant delay with respect to the leading edge. In Figure 12, the doubly diffracted field contributions are marked with the long vertical dotted line. The expected triply diffracted field contributions are marked with the dots just above the waveform. In the deconvolved measurement results, we observe consistent reflections on the expected positions.

An interesting result that can be derived from these observations is the group velocity of the surface wave. The measured velocity is approximately 1.8×0^8 m/s, or 60% of the travelling-wave velocity in vacuum. This dramatic reduction of speed can be explained by the influence of the conducting surface. Additionally, the thin layer of aluminum oxide at the top of the surface can slow the wave down. Additional work is needed on this topic to examine the physics behind these effects.

6.2 Frequency-Domain Results

The frequency-domain RCS is obtained from the time-domain measurements via a Fourier transform. The gated object response is 300 points long, resulting in a frequency resolution of $5 \times 10^9/299 = 0.17$ GHz. To verify the results, they are compared to the calculated RCS of an identically sized plate, and to data obtained from standard frequency-domain measurements.

6.2.1 Comparison of the Measured and Calculated RCS

The RCS of an identically sized flat plate that lacks the artificial roughness (see Section 4.4) is calculated with a high-frequency

model. This model predicted the Physical Optics contribution of the RCS of the object. The calculated results and the transformed time-domain measurements are compared at two frequencies along the antenna bandwidth: 8 and 12 GHz. The results are shown in Figure 17. The measured RCS is normalized. It is observed that the calculated nulls are much deeper than the measured nulls. The reason for this effect is probably that the calculation does not include any diffraction contribution. It is likely that in the measured results, these diffraction contributions have "filled" the deep nulls. Moreover, the presence of noise and clutter in the measurements prevent nulls below the noise floor.

At 8 GHz, the correspondence of the positions and widths of the main lobe and its sidelobes is good. The high RCS level at 90° is caused by the relatively strong reflection contribution from the side area of the plate. The absence of single-diffraction contributions in the calculation could explain the differences between the predicted and measured RCS for angles of incidence between 40° and 60°.

At 12 GHz, there is also a good correspondence of the positions and widths of the main lobe and its sidelobes. The signal-to-noise ratio has decreased, because the power spectral density of the transmitted pulse is lower at higher frequencies. For angles of incidence above 80°, the rough back of the plate becomes optically visible, resulting in a higher-than-predicted RCS.

Figure 18 shows the measured and calculated frequency dependence of the broadside RCS. Because the deconvolution determines the relationship between the frequency components by eliminating the antenna transfer function, this plot is an indication of the deconvolution performance, which is also related to the overall system performance.

This figure shows that the agreement between measurement and prediction is well within the specified antenna limits (2-

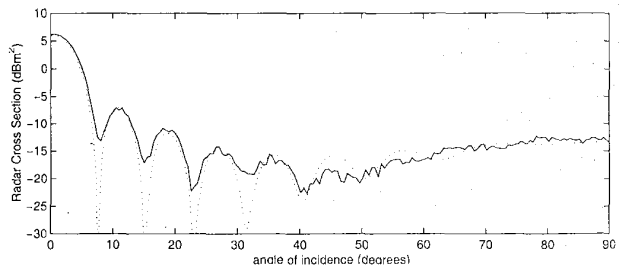

Figure 17a. The calculated (dotted) and measured (solid) RCS of the flat plate at 8 GHz.

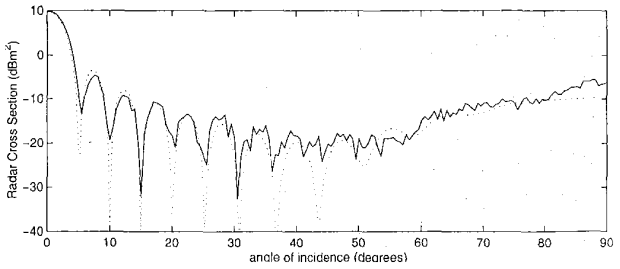

Figure 17b. The calculated (dotted) and measured (solid) RCS of the flat plate at 12 GHz.

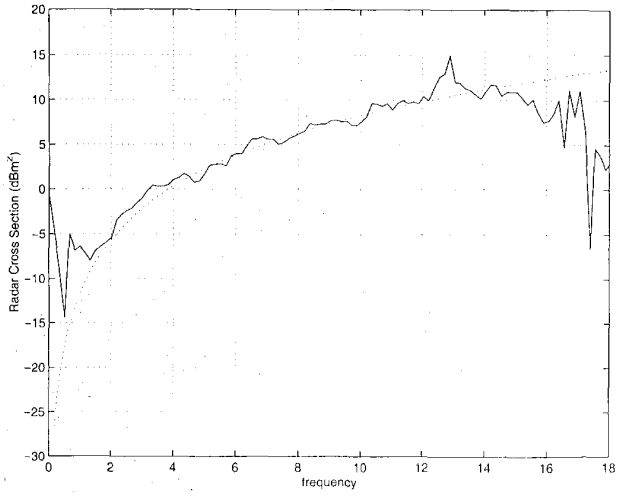

Figure 18. The measured (solid) and calculated (dotted) frequency dependence of the broadside RCS of a flat plate.

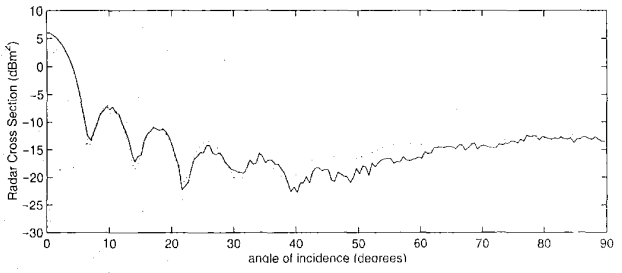

Figure 19a. A comparison of the transformed time-domain measurements (solid) and frequency-domain measurements (dotted) of the flat plate at 8 GHz.

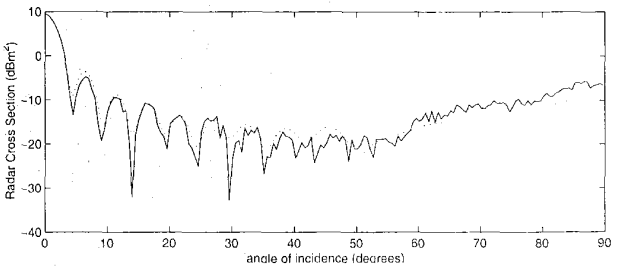

Figure 19b. A comparison of the transformed time-domain measurements (solid) and frequency-domain measurements (dotted) of the flat plate at 12 GHz.

12 GHz). The maximum error is 2 dB. Additional examination of the measurement system must reveal the source of this error and how it can be reduced.

6.2.2 Comparison of Time and Frequency-Domain Measurements

The transformed time-domain measurements are also compared to frequency-domain measurements from Pieper [15]. These

measurements were performed in the same anechoic chamber and with the same flat plate. The main difference between the measurements are the antennas used. Both results are shown in Figure 19. Note that the time-domain measurements are normalized with respect to the frequency-domain measurements, because no absolute calibration measurement is performed for the ridged-horn antennas. Apart from the small differences between 40° and 60°, the agreement is good.

The signal-to-noise ratio of the time-domain measurements is less than the frequency-domain SNR. However, several measured effects cannot be explained by the lower SNR, for example, the relatively low RCS between 40° and 60° at 8 GHz.

7. Conclusions

In this paper, we have demonstrated several potentials of time-domain electromagnetic scattering measurements. This time-domain technique offers operational advantages (direct gating, simple and relatively cheap measurement setup, and reduction of the measurement time, thereby reducing the measurement costs), as well as functional advantages (large instantaneous bandwidth). The range resolution (after software processing) is very high (100 ps). The RCS of a flat metal plate is determined with the time-domain setup. The high range resolution allows us to distinguish several scattering mechanisms of the flat plate, such as the specular reflection, and single, double, and triple diffraction.

8. Acknowledgements

The authors are very grateful to L. J. van Ewijk, from the Physics and Electronics Laboratory of the Netherlands Organization for Applied Scientific Research (TNO-FEL), for providing the *RAPPORT* (Radar signature Analysis and Prediction by Physical Optics and Ray Tracing) RCS calculations.

9. References

1. Peter J.F. Swart and Paul Snoeij, "Point Target Simulation Verification Using Low Level RCS Measurements," 1991 International Geoscience and Remote Sensing Symposium IGARSS91, 1991.

2. Paul Snoeij and Peter J. F. Swart, "Theoretical Prediction and Measurement of the Scattering from Thin Wires with One-Dimensional Random Orientation" 1994 International Geoscience and Remote Sensing Symposium IGARSS94, 1994.

3. Rene V. de Jongh, "The Fundamentals of Time Domain Antenna Measurement," Technical Report IRCTR-S-001.96, International Research Centre for Telecommunication -transmission and Radar," July 1996.

4. Rene V. de Jongh, M. Hajian, and L. P. Ligthart, "Antenna Time-Domain Measurement Techniques," *IEEE Antennas and Propagation Magazine*, **39**, 5, October 1997, pp. 7-12.

5. H. L. Bertoni, L. Carin, and L. B. Felsen (eds.), *Ultra-Wideband, Short-Pulse Electromagnetics*, New York, Plenum Press, 1993.

6. Wim A. van Cappellen, "Ultra-Short Pulse Time Domain Radar Cross Section Measurements," MS thesis, Delft University of Technology, July 1998; available at http://irctr.et.tudelft.nl/reports/.

7. Merrill I. Skolnik, *Introduction to Radar Systems*, New York, McGraw-Hill, 1980.

8. Constantine A. Balanis, *Antenna Theory, Analysis and Design*, New York, John Wiley & Sons, 1982.

9. Amir Shlivinski, Ehud Heyman, and Raphael Kastner, "Antenna Characterization in the Time Domain," *IEEE Transactions on Antennas and Propagation*, **AP-45**, 7, July 1997.

10. Wouter J. C. Pieper, "The Calculation and Measurement of the Microwave Scattering from Artificial Rough Surfaces," *Proceedings of the 7th URSI Commission F Open Symposium*, November 1995.

11. Edward J. Rothwell and Weimin Sun, "Time Domain Deconvolution of Transient Radar Data," *IEEE Transactions on Antennas and Propagation*, **AP-38**, 4, April 1990.

12. G. Hayward and J. E. Lewis, "Comparison of Some Non-Adaptive Deconvolution Techniques for Resolution Enhancement of Ultrasonic Data," *Ultrasonics*, May 1988.

13. M. P. Ekstrom, "A Spectral Characterization of the Ill-Conditioning in Numerical Deconvolution," *IEEE Transactions on Audio and Electroacoustics*, August 1973.

14. Jahangir Rahman and Tapan Sarkar, "Deconvolution and Total Least Squares in Finding the Impulse Response of an Electromagnetic System from Measured Data," *IEEE Transactions on Antennas and Propagation*, **AP-43**, 4, April 1995.

15. Wouter J. C. Pieper, "Scattering from an Artificial Rough Surface, Calculation and Measurement," MS thesis, Delft University of Technology, December 1995.

Introducing Feature Article Authors

Wim van Cappellen was born in Hilversum on February 11, 1975. In 1998, he graduated cum laude in the subject of time-

domain radar cross section measurements. Currently, he is employed at Hollandse Signaalapparaten BV as a radar researcher in naval radar systems. His professional areas of interest include time-domain electromagnetic measurements and radar system design.

René de Jongh was born on January 16, 1971. In 1994, he received a MS degree in Electrical Engineering from Delft University of Technology. In 1996, he completed a post-graduate designer course at Delft University of Technology, and was registered as a "chartered designer" at the Royal Dutch Association of Engineers (KIVI). The designer course comprised the implementation and verification of time-domain antenna measurements. From 1996 until 1998, he worked as a researcher on the development of improved ground-penetrating radar (GPR) systems. Currently, Ren de Jongh is working for Hollandse Signaalapparaten BV in the field of naval radar systems.

Mr. de Jongh's professional interests include the areas of broadband antennas, radar system design, and the application of the time-domain method in microwave measurements. He is currently involved in the development of shared-aperture systems for the next generation of naval ships.

Leo P. Ligthart was born on September 15, 1946. He has been Director of the International Research Centre for Telecommunications-transmission and Radar (IRCTR) since 1994, and has been a Professor in "Microwave transmission, Radar and Remote Sensing," Delft University of Technology since 1992. He first joined the university as a student assistant, scientist, and Professor in "Radar." He holds the Doctor of Technology degree from Delft University of Technology, and the Engineers degree cum laude.

Prof. Ligthart's principal areas of specialization include antennas and propagation, radar, and remote sensing, but he has also been active in satellite, mobile, and radio communications. He is currently working on radio propagation, multi-function antennas, radar remote sensing of the Earth and the atmosphere, multi-parameter radar, and radar networking.

Prof. Ligthart is Fellow of the IEE, a member of IEE professional group E11, and a Senior Member of the IEEE. He chairs the National Platform Telecommunication Transmission and Radar (TTR), Utilization Committees, and manages projects with support of the National Technology Foundation. He represents the Netherlands on URSI Commission F, EU/COST Telecommunication projects, and Advanced Weather Radar. He has published over 150 papers, and was honored with the Veder award in 1981, the IEE Blumlein-Brown Williams Premium in 1982, and he received the Doctor Honoris Causa at Moscow State Technical University of Civil Aviation in 1999.

Editor's Comments *Continued from page 8*

response measurement, and to use deconvolution to recover the response of the object being illuminated. The authors show how to do this, and illustrate the process with a simple experiment. The results agree well with both theory and with measured frequency-domain data. They also clearly illustrate the ability of the technique to separate various scattering mechanisms associated with the target.

There is a tremendous amount of research and development in our field that was done in the former Soviet Union, but which is only now becoming known in the rest of the world. The feature article by Orest Vendik and Yuri Yegorov describes some of this work: in particular, the development of the first phased-array antenna in Russia. It is a very interesting antenna: an array of dielectric-rod antennas, fed through ferrite phase shifters. The article provides a fascinating look at the process involved in the antenna's development, and at the related work that followed its development. I think you'll enjoy reading it. I really appreciate the authors' efforts in preparing this article, and in sharing it with us. Unfortunately, Yuri Yegorov died shortly before the article was submitted. We remember him with its publication.

Designing an antenna for operation across all or a significant portion of the HF band is a true challenge. The classic approach to this problem, invented almost 60 years ago, is the trapped-wire antenna. Inductor-capacitor traps are inserted into a wire antenna designed for the lowest frequency to be covered. These traps permit operation of the antenna at a series of discrete bands of frequencies. However, most such designs require that the frequency bands of operation be sufficiently different from the resonant frequencies of the traps so that interference does not occur. In their feature article, Daniel Reuster and Kevin Cybert describe a new version of this type of antenna. The difference is that the new design permits the frequencies in the bands of operation of the trapped segments of the antenna to overlap, providing continuous coverage over a much wider band of frequencies. The new design also permits better control of the pattern of the antenna, eliminating significant pattern lobes that are normally a consequence of such antenna designs. The design of the antenna is described, and the predicted performance is compared to measured data obtained from two prototypes.

One of the most important aspects of a cellular communication system is how it handles power control. This has tremendous economic impact: it can determine how many mobile users a single cell can support, and it can have a major effect on battery life in the handset. In their contribution to Christos Christodoulou's and Tuli Herscovici's Wireless Corner, Aly El-Osery and Chaouki Abdallah describe a method of distributed power control for CDMA systems. If you have any interest in cellular communications, you should read this: it's both an excellent introduction to an important topic, and a valuable new solution to the problem.

The Uniform Computer Information Transaction Act is a piece of legislation that can be horrible for anyone who purchases a license for computer software, or who pays to have computer software written. Unfortunately, UCITA has become law in several US states, and is under consideration in many others. You need to be aware of what is going on here. Read Merrill Buckley's IEEE–USA column to find out.

Two of our feature articles deal with antennas and propagation at relatively low frequencies. An antenna for use at a wave-

Continued on page 131